communications earth & environment

Article

https://doi.org/10.1038/s43247-024-01304-y

# The complex composition of organic aerosols emitted during burning varies between Arctic and boreal peat



Eric Schneider[1,2], Christopher P. Rüger[1,2] ✉, Martha L. Chacón-Patiño[3], Markus Somero[4], Meri M. Ruppel[5], Mika Ihalainen[4], Kajar Köster[4], Olli Sippula[4,6], Hendryk Czech[1,7] ✉ & Ralf Zimmermann[1,2,7]

Peatlands in the northern hemisphere are a major carbon storage but face an increased risk of wildfires due to climate change leading to large-scale smoldering fires in boreal and Arctic peatlands. Smoldering fires release organic carbon rich particulate matter, which influences the earth's radiative balance and can cause adverse health effects for humans. Here we characterize the molecular composition of biomass burning particulate matter generated by laboratory burning experiments of peat by electrospray ionization 21 T Fourier-transform ion cyclotron resonance mass spectrometry, revealing a highly complex mixture of aromatic and aliphatic organic compounds with abundant heteroatoms including oxygen, sulfur and up to five nitrogen atoms. Primary organosulfur species are identified in the emissions of peat-smoldering, in part also containing nitrogen. Differences are observed when comparing structural motifs as well as the chemical composition of boreal and Arctic peat burning emissions, with the latter containing compounds with more nitrogen and sulfur.

Peatlands are formed through incomplete plant decomposition and consequential accumulation of biomass under waterlogged conditions. Globally, they are estimated to store 500–600 Gt of carbon, representing one-third of terrestrial organic carbon (OC) [1–3].

Boreal peatlands cover the largest area of peatlands worldwide and are home to a large variety of vascular and non-vascular plants that form the peat layer over time, especially, various species of *Sphagnum* mosses, sedges, and shrubs[4]. The vegetation of a peatland is dependent on the availability of nutrients, but also on the climatic conditions, most importantly the moisture balance, and surface topography leading to minerotrophic mires and ombrotrophic bogs hosting different plant and microbial communities. Peatlands are also abundant in the Arctic, where permafrost can occur, forming an ice-rich foundation and a shallow active layer where vegetation and accumulation of organic matter are possible in the summer months[5]. With increasing depth of the peat layer, the maturation of fresh biomass increases due to methanogenesis under anaerobic conditions, consequently forming fossilized materials like lignite by coalification[6].

Climate change, resulting in increased average temperatures and large-scale peatland drying, leads to thawing of permafrost peatlands and desiccation of boreal and Arctic peatlands, which is additionally amplified by human activity, such as commercial peat harvesting, drainage for agriculture and forestry, and road construction[1,7]. Peatland degradation leads to increased greenhouse gas (GHG) emissions from peatlands[8,9], as well as increased risk of large-scale peat fires, further amplified by climate change-related increased peat fire ignition by lightning[10]. Consequently, emitting extensive amounts of GHG and particulate matter (PM) into the atmosphere and causing regional haze events[7,11,12]. GHG emissions from peat fires have been estimated to match ~15% of anthropogenic emissions, creating a positive feedback loop accelerating global warming[13]. As Arctic permafrost peatlands are located in regions that undergo the most rapid changes due to climate warming[14], large-scale peatland fires may occur more often and at new, more northern, locations that have previously not been threatened by wildfires, introducing thawed permafrost peat as a new type of wildfire fuel[15,16]. While peatland fires have occurred since the last ice age[17], Arctic

[1]Joint Mass Spectrometry Centre, Department of Analytical and Technical Chemistry, University of Rostock, Rostock, Germany. [2]Department Life, Light & Matter (LL&M), University of Rostock, Rostock, Germany. [3]National High Magnetic Field Laboratory, Florida State University, Tallahassee, FL, USA. [4]Department of Environmental and Biological Sciences, University of Eastern Finland, Kuopio, Finland. [5]Atmospheric Composition Unit, Finnish Meteorological Institute, Helsinki, Finland. [6]Department of Chemistry, University of Eastern Finland, Joensuu, Finland. [7]Joint Mass Spectrometry Centre, Cooperation Group "Comprehensive Molecular Analytics" (CMA), Helmholtz Centre Munich, Munich, Germany. ✉e-mail: christopher.rueger@uni-rostock.de; hendryk.czech@uni-rostock.de

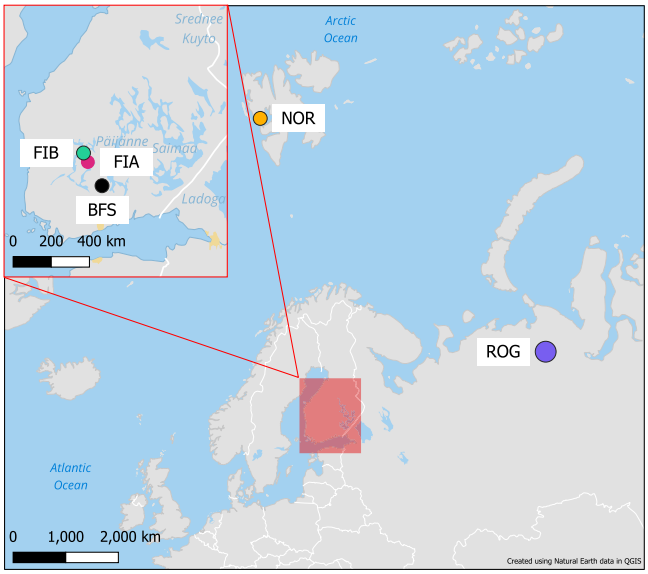


**Fig. 1 | Map of sampling locations.** Map indicating the origin of each peat sample (FIA: Lakkasuo, FIB: Siikaneva, ROG: Rogovaya, NOR: Svalbard and the boreal forest surface (BFS) sample. Map created using the Free and Open Source QGIS.

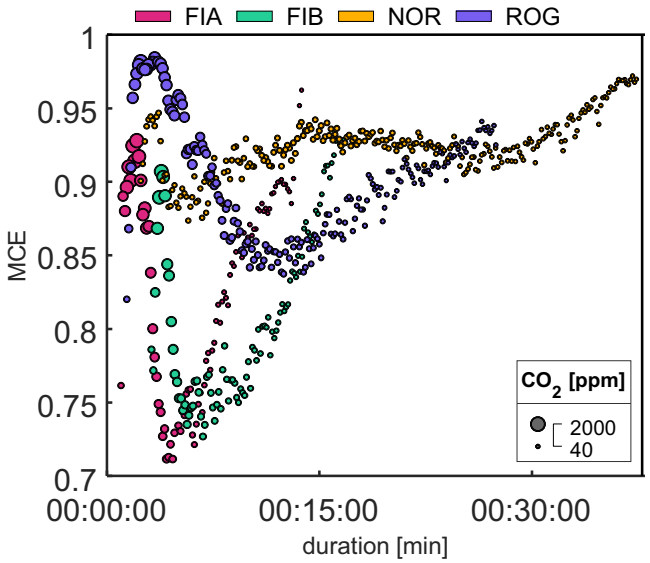


**Fig. 2 | Combustion efficiency during sampling.** Time-resolved modified combustion efficiency (MCE) for each peat combustion experiment starting at the timepoint of the first visible flame. The dot size indicates the concentration of emitted $CO_2$ in the flue gas stack. The $CO_2$ concentrations are proportional to the combustion rate, with high values indicating high combustion intensity.

peatland fires have only recently been recognized as an emerging threat, with unforeseen areas burning in recent years. Currently, limited information is available on these fires as well as the emitted particles[10,16,18,19].

Peatlands are typically affected by smoldering fires which are characterized by slow, flameless burning at low temperatures (max. 450–700 °C) with heterogeneous oxidation taking place between the solid phase and airborne oxidants, whereas flaming combustion at higher temperatures involves fuel volatilization and subsequent homogeneous oxidation in the gas phase[20,21]. Peatland wildfires can continue smoldering underground in deep organic soils for extended periods, propagating horizontally and vertically, consequently affecting large areas, and potentially starting new fires long after the initial wildfire, even overwintering at air temperatures below −35 °C[18,22,23].

Smoldering combustion leads to the formation of large quantities of PM rich in OC and poor in elemental carbon (EC)[24]. Adverse health effects due to peat wildfires have been observed in population-based epidemiologic studies[25,26], as well as in animal studies showing a cardiovascular response[27,28].

Emissions from biomass burning (BB), including peat, are the main source of light-absorbing OC (also called brown carbon (BrC)) to the atmosphere[29]. High BrC emissions have been reported, especially from smoldering combustion of peat[24,30,31]. The strong absorptivity of BrC from boreal peatland fires was shown to result in positive net forcing over bright surfaces[24] and peat smoldering fires were found to emit brown carbonaceous "tar balls", a known type of light-absorbing particles from BB[15,32]. Therefore, the molecular characterization of these compounds is of particular interest.

Beyond absorption of visible UV light, properties like volatility and hygroscopicity are dictated by the organic aerosol composition, affecting its fate and impact on processes during atmospheric residence. The hygroscopicity of PM influences its ability to act as cloud condensation nuclei (CCN), e.g., organosulfates have been found to increase the water uptake even at sub-saturated relative humidity while also increasing particle acidity and viscosity[33–35] and consequently, secondary reactions may take place in the aqueous phase leading to the formation or degradation of organic aerosol compounds[36].

Electrospray ionization (ESI) 21 T Fourier-transform ion cyclotron resonance mass spectrometry (FT-ICR MS) is applied in this study, to characterize the highly complex mixture of smoldering peat burning organic aerosol and its influence on earth's radiative balance as well as indications for the explanation of adverse health effects induced by peatland fire emissions. Additionally, better understanding of the emitted organic aerosol is an important factor to facilitate distinguishing boreal and Arctic peat fires from each other as well as from other emission sources, e.g., boreal forest fires. Utilizing the unique, advanced capabilities of a 21 T FT-ICR MS[37], regarding mass accuracy, resolving power[38,39] and dynamic range[40], this system enables the identification of tens of thousands of compounds up to high mass (1200 Da) and high heteroatom content, including organosulfur and organonitrogen species. Additional certainty of sum formula assignment is achieved by fine isotopic fingerprint matching[41]. The characterization of the emitted peat-burning organic aerosol further increases in relevance as high-latitude fires increase due to climate change.

## Results and discussion

### Combustion conditions

Each Biomass sample (Fig. 1) was ignited the same way (as described in "Sampling sites and laboratory burning experiments"), and therefore the combustion behavior and the resulting emissions are an intrinsic property of the respective samples. Peat combustion was predominantly characterized by smoldering, with only short phases of flaming. The average MCE values of each combustion is in the range of 0.82–0.92, which is in good agreement with MCE values reported in other peat fire emission studies[7]. The two Finnish peat samples (FIA, FIB) show the lowest MCE value, close to 0.8, which is commonly considered an indication of smoldering combustion[42]. The two permafrost peat samples (ROG, NOR) show a higher MCE value of around 0.9, indicating smoldering as well as flaming, which was also visually observed for short periods. In addition to the MCE, the duration and the intensity of the combustion is also different for each sample (Fig. 2, Supplementary Table 1). During the experiments, peat samples were burned quickly from start to finish, with the exception of NOR for which the ignition was clearly slower than for the other peat samples, and only small flames were visible, which is reflected in comparably low concentrations of emitted $CO_2$. FIA burned the fastest (12 min), followed by FIB, NOR, and ROG (24–33 min), while BFS was burning much longer (55 min) as a result of its larger initial sample mass. Due to the unique location of the NOR sampling site, this sample was the only one to include significant amounts of mineral material in the peat profile, leading to the poorest combustion quality and a high residual mass fraction in the thermal analysis of the peat (Supplementary Table 5). Differences in plant composition as well as lower microbial activity in permafrost peatlands may also explain the higher MCE

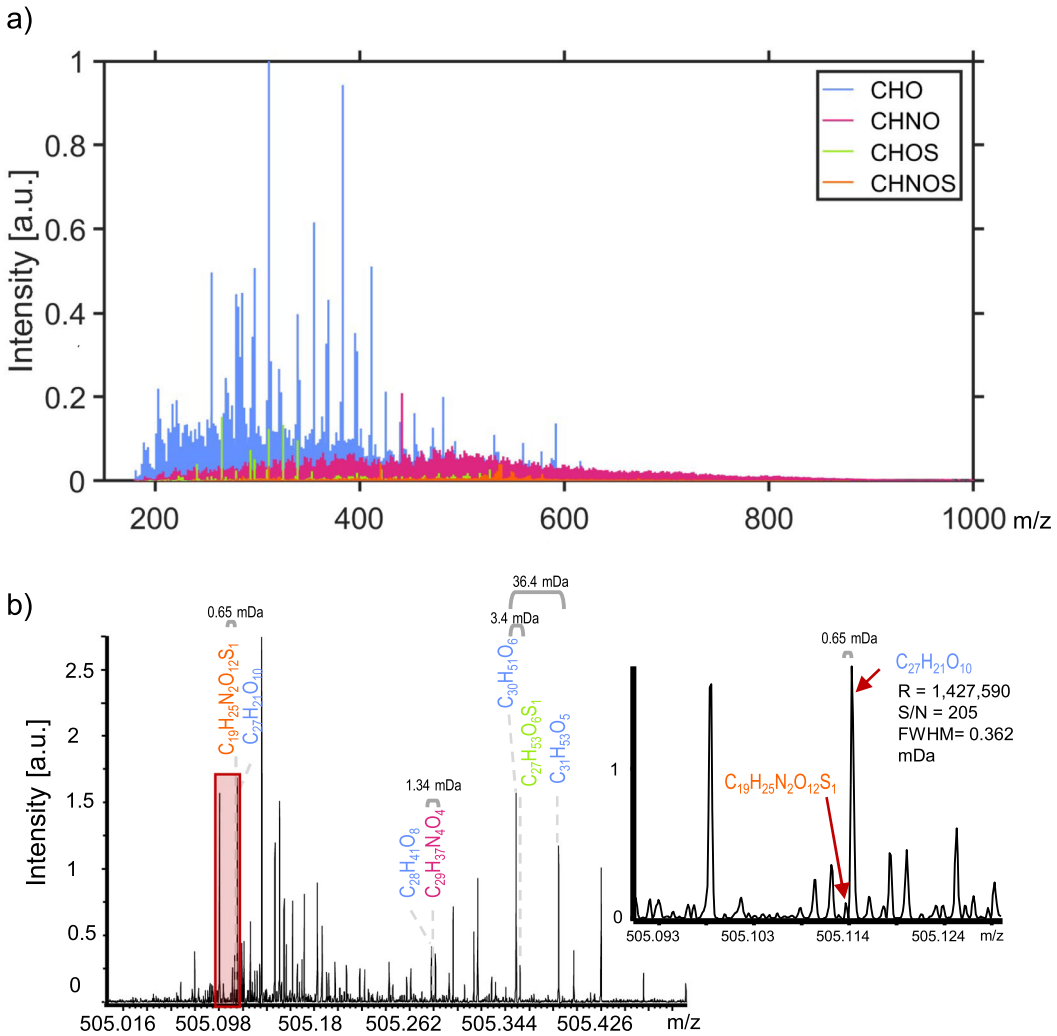


**Fig. 3 | Ultrahigh-resolution mass spectra of assigned compounds in organic peat-smoldering aerosol. a** Mass spectrum of assigned elemental compositions in sample FIB by ESI(−) 21 T FT-ICR MS color-coded by compound class. **b** Zoom-ins on one nominal mass (*m/z* 505–505.5) including 115 resolved peaks, highlighting the need for ultrahigh resolving power, dynamic range, and mass accuracy to handle the extreme molecular complexity, e.g., for resolving indicated minuscule mass splits over the whole mass range.

values of NOR and ROG, due to lower degradation of the biomass, especially lower degradation of aliphatic compounds and aliphatic sidechains, which are one target of microbial decomposition[43,44]. As aliphatic compounds possess a lower ignition temperature than, e.g., aromatic ring structures[45], a higher abundance of these compounds may lead to a higher ratio of $CO_2$ to CO and, therefore, higher MCE values.

### Application of advanced mass spectrometry

Smoldering combustion conditions in BB have been characterized to release large amounts of incomplete thermal degradation products[24], with the elemental composition and, to some extent, the molecular structure of organic aerosol compounds reflecting the chemical composition and molecular structure of the respective fuel[46]. Therefore, under similar combustion conditions, a chemically more complex biomass, like peat, is expected to produce a more complex organic aerosol mixture than a less complex biomass, e.g., logwood.

All filter extracts analyzed by ESI 21 T FT-ICR MS showed an extreme molecular complexity with up to 28,000 and 45,000 assigned monoisotopic elemental compositions in negative and positive mode ESI, respectively. The increased dynamic range (difference of highest and lowest detectable peak intensity), resulting from the higher magnetic field in the FT-ICR cell[47], enables the detection of more low-intensity compounds that would otherwise be missed due to suppression by high-intensity signals, e.g., from the $CHO_X$ or $CHN_{1\text{-}2}O_X$ class (Fig. 3a)[48]. In addition to the dynamic range (ESI(−): 809–3,235 and ESI(+): 103–508), the resolving power of an FT-ICR instrument is also, among other parameters[49], increased by the magnetic field strength ($R = 1.7$ million at *m/z* 400, R = 850,000 at *m/z* 800). Likewise, the lowest non-coalesced mass is increased with increasing magnetic field strength, enabling the differentiation of ion clouds in the ICR cell with small *m/z* differences even at high *m/z* and ion numbers in the cell[50].

For complex peat organic aerosol analysis, a high mass resolution is necessary to resolve adjacent peaks in the mass spectrum, as combinations of several heteroelements (O, N, S, P) can result in sub-mDa exact mass differences (mass splits), which need to be resolved for accurate peak picking and sum formula assignment. While resolving commonly observed mass splits (Fig. 3b) like $CH_4/O_1$ (36.4 mDa), $CH_2/N_1$ (12.6 mDa) or $C_3/SH_4$ (3.4 mDa), even at higher masses (500–1000 Da), is not challenging for most FT-ICR MS systems (Supplementary Fig. 1), less common mass splits like $H_4O_4/C_1N_4$ (1.34 mDa), $C_8/H_4N_2O_2S_1$ (0.65 mDa) or $C_{14}/H_5N_2O_7Na_1$ (0.56 mDa) call for higher resolving power as provided by 21 T FT-ICR MS. Additionally, high mass accuracy of the 21 T FT-ICR MS (error <200 ppb, RMSE < 60 ppb) results in increased confidence for sum formula assignment and also enables verification of assigned elemental compositions by their unique fine isotopic structure[51,52].

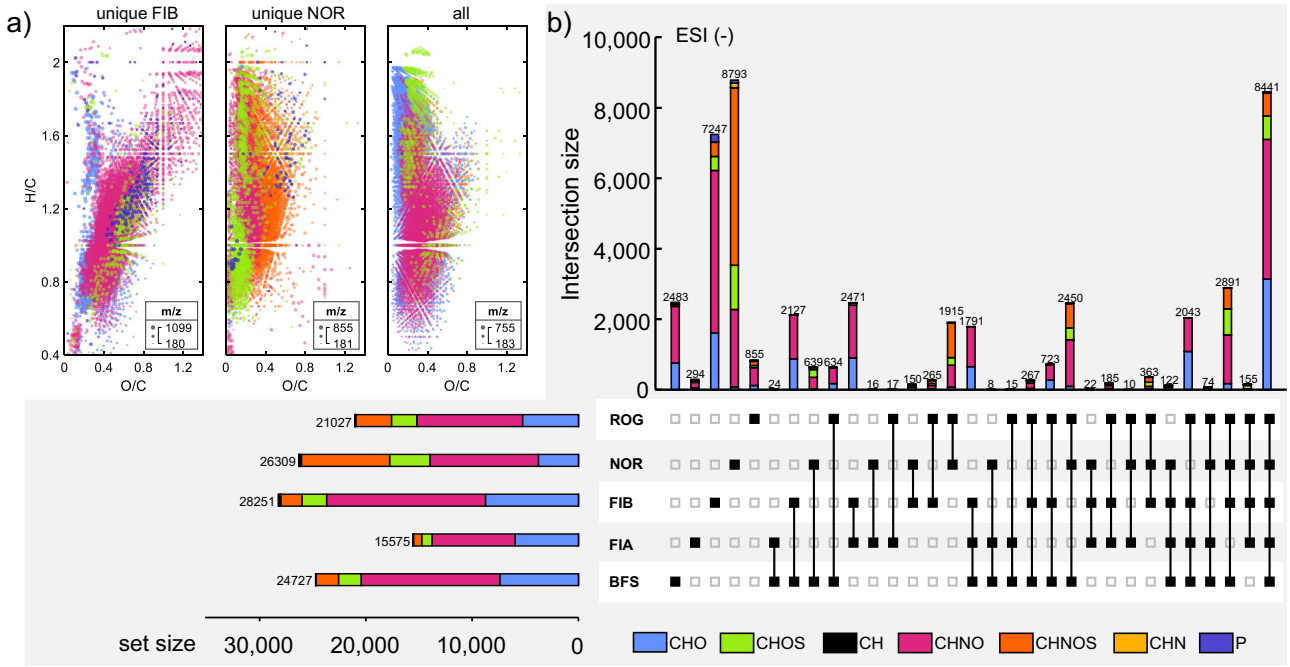


**Fig. 4 | Molecular-level comparison of detected elemental compositions. a** Van Krevelen diagrams of oxygen-containing compounds in selected ESI(−) upset plot intersections (unique FIB, unique NOR and all) with *m/z* indicated by dot size and compound class indicated by color. **b** Upset plot of five organic aerosol extract ESI(−) datasets with compound class distribution in the whole dataset (bottom left) and the individual intersections (top right) indicated by color (CHO light blue, CHOS green, CH black, CHNO magenta, CHNOS orange, CHN yellow, *P* (sum of CHOP and CHNOP) dark blue).

The ultrahigh-resolution analysis of peat combustion organic aerosol samples identified a broad distribution of oxidized compounds, often containing at least one and up to five nitrogen atoms, as well as some abundance of up to one sulfur atom and a minor occurrence of phosphorous, in the mass range of 180–1100 Da (Supplementary Table 6). Especially for the most abundant CHO and CHNO compound classes (ESI +/−: 92–97%/53–88% rel. number and 84–98%/66–92% rel. intensity), the oxygen number distribution pattern covers the whole range from 1–20 or more oxygen atoms per molecule (Supplementary Figs. 2, 3a, c). This pattern remains stable when increasing the number of nitrogen atoms per molecule, also when comparing the relative differences between samples, e.g., ESI (−) FIB shows the highest number of formulae with $x > 10$ oxygen atoms in the $CHO_X$ and $CHN_{1\text{-}3}O_X$ compound classes. Both compound classes are characterized by mostly (poly-)phenol-like structures, with some addition of polycyclic aromatic hydrocarbon (PAH) like and aliphatic-like structures, classified by their modified aromaticity index and H/C ratio (Supplementary Figs. 2, 3b, d)[53]. The observed oxygen distribution pattern is a result of the incomplete smoldering combustion of peat, dictated by the low availability of oxygen and low temperatures. The abundance of (poly-) phenol-like compounds, as a degradation product of larger biomass structures (e.g., lignin, cellulose, hemicellulose), is a typical observation in BB[46], resulting in common BB marker compounds with characteristic concentration ratios determined by the respective type of biomass[54]. Still, primary peat smoldering emissions showed an unusually high number of nitrogen-containing compounds with $\#N > 3$, as well as organosulfur and nitrogen-containing organosulfur compounds (Supplementary Figs. 2, 3e, g), which are not typically identified in primary BB emissions. The abundance and distribution of these compounds vary in each peat aerosol sample, highlighting the importance of combustion conditions as well as the environmental conditions at the peatlands, influencing the peat composition.

### Effect of peat origin on organic aerosol composition

Comparing datasets from each peat location reveals both distinct differences and similarities of detected elemental compositions (Fig. 4 and Supplementary Fig. 4). For both ESI polarities, a comparable behavior of intersection sizes between each dataset is observed, with the intersection including all datasets among the top three most populated intersections, together with unique NOR and unique FIB elemental compositions. Additionally, a significant overlap is found between datasets of the two Finnish peat samples (FIA, FIB), as well as FIB with the boreal forest surface (BFS) and the ROG sample. The dataset of NOR, which was correctly expected to be the most unique sample due to its sampling environment, shows its strongest overlap with ROG and BFS. The sample BFS seems to contain significant numbers of compounds that are found in either the Finnish peat samples the permafrost peat samples, or both. This may be explained by the structure of the BFS, containing both, partially decomposed biomass in the lower layers as well as debris, moss, and grasses in the top layer of the soil, which also leads to a mix of combustion conditions of smoldering in the lower layers and flaming of the top layer. Results from this in-depth analysis are therefore useful to help distinguish between boreal forest and boreal and Arctic/permafrost peat fires, as peat fires emit a large number of unique compounds, not found in BFS fires.

In ESI(+) the majority of detected elemental compositions contain nitrogen, but especially intersections including ROG and NOR contain mostly nitrogen-containing compounds, and almost all detected CHN compounds are shared with the ROG or NOR dataset. The same statement holds for sulfur-containing compounds and nitrogen- and sulfur-containing compounds in ESI(−). The NOR (−) dataset includes 45% CHOS and CHNOS compounds, which are, to a large extent, unique for this dataset, but some are also shared with ROG and the other samples. These compounds are predominantly detected in ESI(−), with only a minor abundance in FIB (+) and NOR (+), and always with a high O/S ratio (O/S > 7, Supplementary Table 7) and are therefore expected to contain sulfite ($SO_3$), sulfate ($SO_4$) or sulfonic ($HSO_3$) functional groups[41,55]. Overall, the elemental compositions identified in ROG show a large overlap to NOR (77.5% number/94.6% intensity), and likewise FIA shows a large overlap to FIB (92.2% number/98.9% intensity), which in both cases indicated by the low number of unique compounds and the high overlap with the corresponding sample from permafrost or boreal peat, respectively.

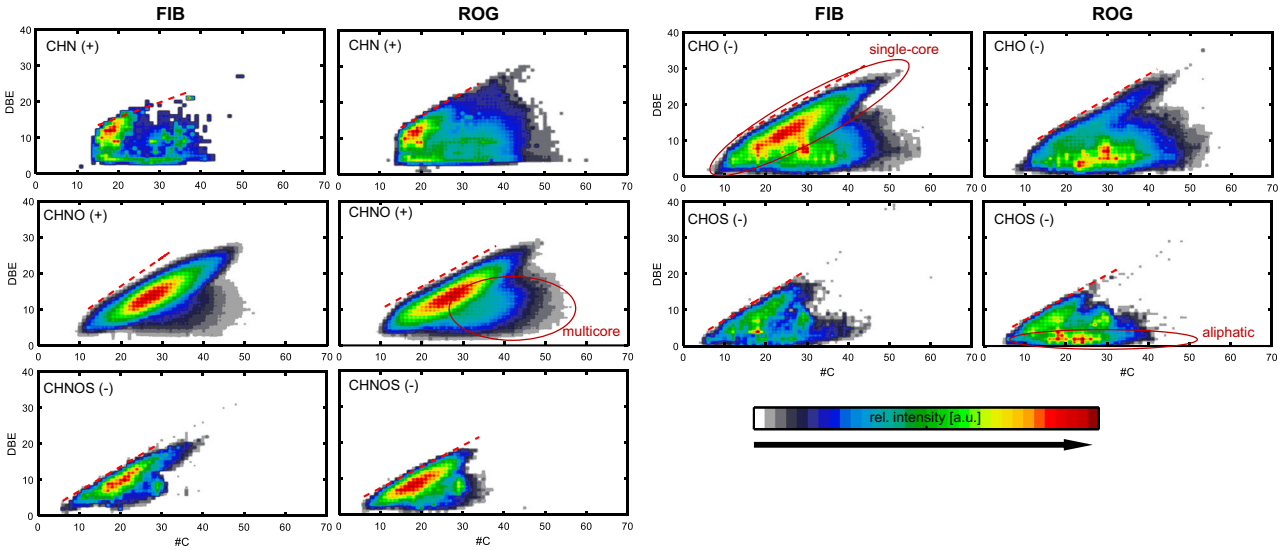


**Fig. 5 | Compound class separated contour plots of double bond equivalent versus carbon number plots.** Contour double bond equivalent (DBE) versus carbon number (#C) plots for CHN(+), CHNO(+), CHNOS(−), CHO(−), and CHOS(−) compound classes in peat burning aerosol extracts from boreal: FIB (left) and Arctic: ROG (right) environments. Compound classes represent the entirety of compounds with their respective heteroatoms. A red dotted line indicates the planar limit of each compound class with a consistent slope of ~0.61.

When comparing Van Krevelen diagrams of unique elemental compositions of FIB(−) and NOR(−) with common compounds (Fig. 4a), NOR(−) shows a broad distribution of nitrogen- and sulfur-containing compounds between H/C = 0.6–2 and O/C = 0–0.5, while FIB(−) shows an ellipse-shaped distribution with moderate to high O/C ratios in the chemical space of phenol-like compounds, which were also observed as main products of *Sphagnum* moss decay in soil organic matter (SOM) analysis of a permafrost bog[56]. The high abundance of nitrogen-containing species in NOR is likely a result of the unique location of the peatland, close to a bird cliff ("Combustion conditions"), which increases the nitrogen content in the peat and consequently in the emitted PM (Supplementary Table 1)[57]. Both intersections also contain a small number of organophosphorus compounds (CHOP and $CHN_1OP$), which have previously also been characterized by ESI(−) 21 T FT-ICR MS analysis of wildfire smoke, but with higher H/C ratios[41]. Both Finnish samples show the broadest oxygen number distribution (Supplementary Fig. 2, 3a, c). Due to the described similarities and considering the combustion conditions section 3.1, primary organic aerosol from the boreal peatlands (FIA, FIB), BFS, and the permafrost peatlands (ROG, NOR) can be clearly distinguished by their chemical composition.

In addition to the elemental composition, also structural information of organic aerosol compounds is of interest for determining the physical-chemical properties of a molecule and, consequently, the aerosol, e.g., regarding light-absorption or hygroscopicity. Mass spectrometric data, without additional chromatographic separation or fragmentation, has limited capabilities for characterizing molecular structures. Nevertheless, the sum formula assignment enabled by UHRMS allows for the calculation of different molecular properties, which may also give insights into the properties and general structural motifs of the organic aerosols.

Calculated saturation vapor pressure (C*) averaged for each compound class (Supplementary Table 8) classifies the detected oxygen-containing compounds in the low and extremely low volatility classes (log(C*) = −4.5–−13), with decreasing volatility correlating to increased hetero-atom numbers[58,59]. Previous studies comparing the combustion of boreal and sub-tropical peat revealed that in boreal peat fire emissions a higher portion of intermediate- and semi-volatile primary OC mass (80%) was found in the particle phase compared to sub-tropical peat (60%). This highlights the importance of particle-bound compounds emitted from boreal peat fires[60].

Figure 5 shows the compound class separated DBE versus carbon number plot of a boreal (FIB) and a permafrost peatland (ROG) sample. The distribution of compounds in these plots can be described by three ellipsoid distribution regions, two horizontal and one tilted, with a slope of 0.61. A similar distribution can be observed for the other peat samples (Supplementary Fig. 5). The slope of the tilted area is equivalent in each sample and often the more abundant region, also in ESI(−), but slightly shifted to a lower DBE and carbon number. The slope of the planar limit in the DBE versus carbon number plot is characteristic of the dominant molecular architecture of the unsaturated aromatic moieties[61]. A slope of zero indicates alkylation, and a slope of 0.25 indicates saturated cyclic ring (e.g., hexane) annulation, as no double bonds (ΔDBE = 0) or one ring (ΔDBE = 1, ΔC = 4) are added to the molecule, respectively. The observed slope of 0.61 is lower than the theoretical slope resulting from linear aromatic ring addition ($a$ = 0.75, ΔDBE = 3, ΔC = 4), therefore mixed addition of cyclohexane and benzene rings can be a main building block of detected compounds in this region[62]. The consistency of the observed slope in each compound class highlights the molecular structure similarities of the hydrocarbon backbone, independent of the abundance of heteroelements. Condensed PAHs are known for their toxicity and high carcinogenic potential, therefore structurally similar oxygenated species are of interest for the explanation of adverse health effects observed by peat smoldering aerosol[25,26].

Similar distributions have been previously observed in the chemical characterization of asphaltenes, a highly aromatic solubility fraction of petroleum, which are described as island- (single-core) and archipelago-motifs (multicore)[63,64]. These two main structural types are defined by containing either one condensed aromatic ring structure with minor alkylation of the core (single-core) or several smaller, partially alkylated aromatic ring systems attached to each other by alkyl chains of variable length (multicore). The two observed distributions in peat aerosol may also be assigned to one of these structural motifs. Both, the boreal and the permafrost peatland samples show a combination of both structural motifs, but the abundance of compounds differs. Permafrost peat combustion seems to favor the formation of multicore type compounds, e.g., like the macromolecular structure of lignin, while single-core type compounds are more abundantly formed by the combustion of boreal peat[65]. This difference may be explained by the combustion of the permafrost peat samples, a difference in the chemical composition of the peat itself, e.g., due to lower microbial biodegradation where (linear) aliphatic sidechains are more easily

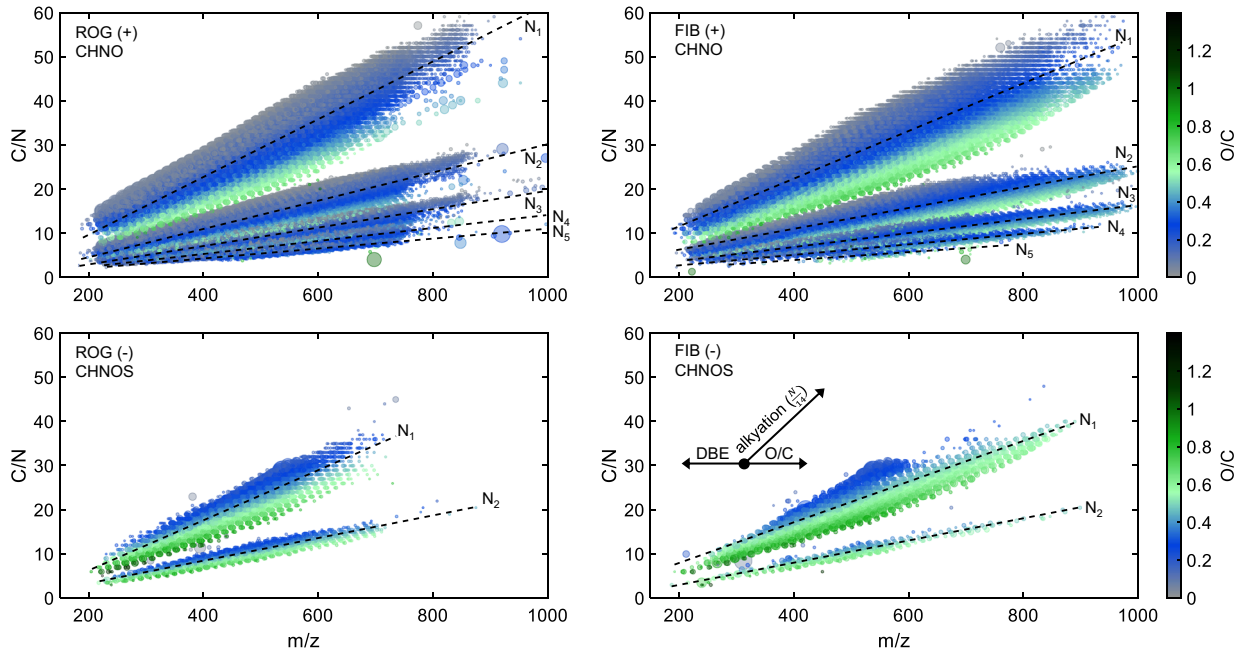


**Fig. 6 | Carbon to nitrogen ratio plots.** Carbon to nitrogen ratios (C/N) versus *m/z* of ROG (left) and FIB (right). The top plots show only CHNO compounds in ESI(+) and the bottom plots show only CHNOS compounds in ESI(−). Black dotted lines indicate linear regression through compounds with the same nitrogen content ($N_{1-5}$, top to bottom).

metabolized than aromatic rings[44,66], or a combined effect of both as the combustion efficiency is inevitably linked to the fuel composition. An increased combustion quality (shorter burn time, lower residual mass of boreal peats FIA and FIB) leads to the loss of aliphatic bridges between archipelago-like aromatic ring systems and, consequently, the formation of larger, island-like aromatic ring systems. Aliphatic-like compounds, e.g., fatty acids, are also more intensely observed in the permafrost peat sample, especially in the CHO- and CHOS- compounds classes, which also refers to more intact biomass structures in the permafrost peat, compared to the boreal peat.

It should be noted that a major difference of peat burning aerosol compared to asphaltenes is the higher heteroatom content, especially oxygen, which may also increase the DBE value of a molecule due to the formation of carbon-oxygen double bonds in carbonyl or carboxyl moieties. Furthermore, the selective ionization of ESI, and differences in the ionization cross sections of the island- and archipelago-type molecules, also need to be considered[67].

### Nitrogen-containing molecules

Alkylated heterocyclic aromatic compounds with one or two nitrogen atoms have been characterized in peat-burning aerosol, e.g., as pyridine derivatives[68,69], but the analysis with ESI 21 T FT-ICR MS reveals a much broader range of compounds, which are of interest due to their potential light-absorbing and ecological effects, e.g., due to the increased water-solubility compared to PAHs[70]. Reduced nitrogen-containing compounds (CHN) in this study are predominantly detected in positive ionization mode (Fig. 5). The negligible abundance of CHN compounds in ESI(−) gives some insights into the molecular structure, as in ESI(−) only acidic moieties, e.g., pyrrole-like or indole-like, would be ionized. The absence of CHN(−) compounds is, therefore, an indicator of the absence of acidic nitrogen-containing structures in these peat aerosol samples. In contrast, ESI(+) shows a broad range of CHN compounds, covering the DBE range as well as extended alkylation with up to five nitrogen atoms, especially for the permafrost peatland samples (NOR, ROG). These compounds likely contain amine or imine moieties, e.g., pyridine derivatives (DBE > 4) or amines (DBE < 4). Reduced nitrogen compounds are a product of volatilization or pyrolysis, as no oxidation is part of the formation process. Still, also under smoldering conditions partial oxidation of compounds must be considered, as well as the presence of nitrogen- and other heteroelement-containing building blocks of the biomass.

Oxidized nitrogen-containing compounds (CHNO) are the most frequently detected compound class in all measurements in both ionization modes, partially due to their effective ionization by ESI. They are detected as condensed aromatic-, phenol- and aliphatic-like structures, similar to CHO compounds without nitrogen (Supplementary Figs. 2, 3d). Figure 6 highlights the broad chemical variety of CHNO compounds detected in peat aerosol samples, exemplary shown for ESI+ data were CHNO compounds are most abundant (CHNO−: Supplementary Fig. 7). Compounds group around one of five lines in the C/N ratio versus *m/z* plot, which correspond to the number of nitrogen atoms ($N_{1-5}$).

When analyzing a hypothetical, symmetrical dataset of alkylated CHNO compounds, a linear regression through each point cloud (each point cloud contains compounds with the same #N) would result in a slope (a) of $a = \#N/14$, as a result of alkylation adding $CH_2$ units increasing the m/z (nominal *m/z* 14) and the C/N by one. The intercept of the theoretical regression would be related to the DBE and #O values, increasing or decreasing the intercept, respectively. For experimental data, the degree of alkylation, oxidation (addition of O, e.g., hydroxyl, carbonyl, carboxyl), and DBE distribution of detected compounds is not constant over the whole mass range. Therefore the slope and intercept of the linear regression line are predominately determined by the shape of the point cloud and not the chemical properties.

The observed shape of point clouds in a sample remains relatively stable when increasing the nitrogen number, with a reduced width dictated by the C/N ratio visualization, indicating a similar distribution of oxygen number and O/C ratio as well as aromaticity, which is the same for compounds detected in both ionization modes.

Distinct differences are likewise observed when comparing linear regressions through compounds with the same number of nitrogen atoms in data of samples from the boreal (FIB) and permafrost (ROG) peatland (likewise: FIA and NOR, Supplementary Fig. 6). Primary smoldering aerosol from permafrost peatlands shows a higher slope and a lower intercept than the boreal peatland samples (Supplementary Table 9). This is explained by a lower O/C ratio at *m/z* > 600 and more abundant low O/C, high DBE

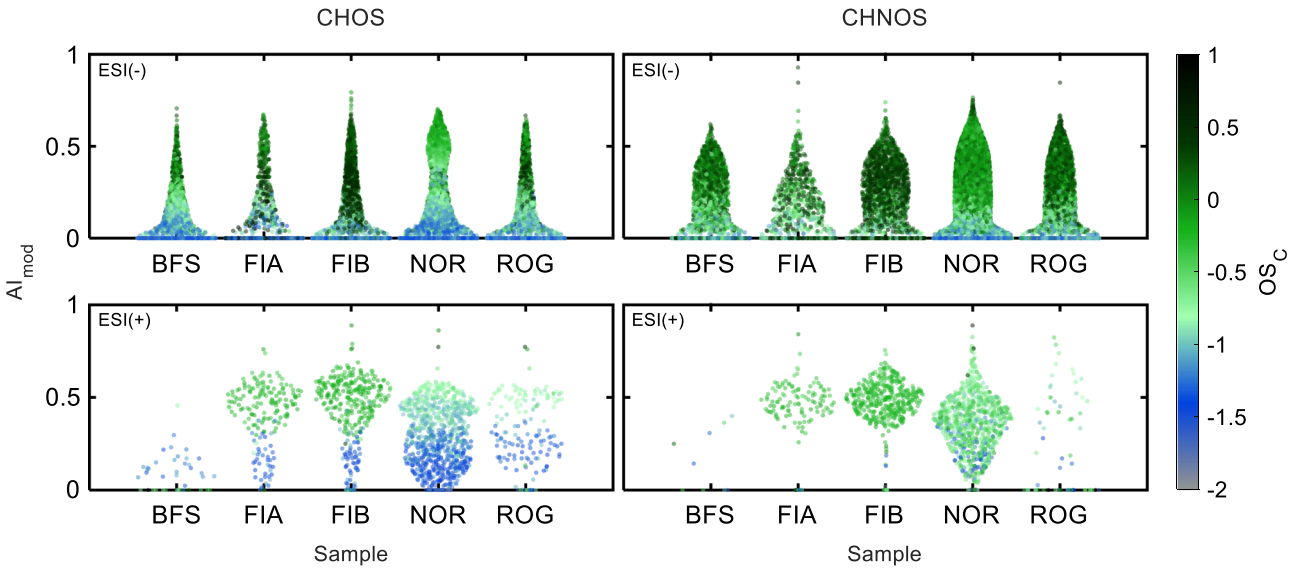


**Fig. 7 | Violin plots of sulfur-containing compounds.** Violin plots of modified aromaticity index ($AI_{mod}$) distribution in CHOS (left) and CHNOS (right) compound classes identified in each peat organic aerosol sample, (ESI(−): top, ESI(+): bottom) with average carbon oxidation state ($OS_C$) indicated by the color bar.

compounds in the range of *m/z* 200−700. CHNO compounds in the permafrost peatland combustion aerosol of this study are less oxidized (lower O/C, lower #O) and more aromatic than their boreal counterparts and additionally show a higher number of compounds containing more than two nitrogen atoms.

Poor combustion quality, in addition to the different composition of peat in permafrost peatlands, generates a distinct chemical profile of organic aerosol compounds, which has a unique effect on the atmospheric interaction of the resulting PM. Molecules with aromatic ring structures combined with nitrogen-containing functional groups have been characterized as strongly light-absorbing species making up a significant part of brown Carbon (BrC)[71]. The formation of these compounds in large-scale permafrost peatland fires has the potential to strongly impact the light-absorbing properties of emitted PM, both in the atmosphere as well as on Arctic snow and ice surfaces.

The high abundance of nitrogen may result from the efficient uptake of atmospherically deposited nitrogen of peat-forming *Sphagnum* mosses, that are found in the vegetation at each sampling site[56,72]. In addition, nitrate-reducing microorganisms have been identified in peatlands which may play a role in the formation of reduced organic nitrogen compounds[56].

Therefore, the distinctively high abundance of nitrogen in single molecules ($N \geq 3$) in combination with a low O/N and O/C ratio could be used to identify primary peatland smoldering emissions in contrast to secondary atmospheric aging products of forest fires that are expected to have a higher O/C and O/N ratio due to nitrate radical-initiated aging, such as dark aging during nighttime or in optically thick wildfire plumes[73–75].

### Sulfur-containing molecules (CHOS & CHNOS)

Organosulfur (OS) compounds are a commonly detected compound class in atmospheric PM samples. They are often detected as organosulfates, but also other oxygenated OS species are reported, including sulfoxides, sulfonates, sulfones, and in their reduced form as e.g., thiophene-like species[76–78]. Their formation was assumed to mainly occur through secondary aerosol chemistry, e.g., by multiphase reactions of organic molecules with acidic sulfate particles or reactions involving gas phase $SO_2$[79,80]. Also, the combination of OS with nitrogen to form e.g., nitrooxy organosulfates has been frequently identified in ambient aerosol at urban sites as well as remote locations like the Arctic, and the formation of these compounds is also assumed to occur through secondary aerosol chemistry[53,78,81].

The investigation of primary peat combustion organic aerosol by ESI (−) 21 T FT-ICR MS reveals a broad variety of CHOS and CHNOS species, covering the entire mass range (Fig. 3a), with high O/S ratios (Supplementary Fig. 2g) including primarily aliphatic but also phenol-like species (Supplementary Fig. 2h). The identification of CHOS and CHNOS compounds in the mass spectra was additionally verified by matching of the experimental data with simulated fine isotopic structures of selected elemental compositions (Supplementary Figs. 8, 9). The fine structure of isotopic peaks is a result of the natural atomic isotope abundance, as most elements in organic compounds have additional isotopes, e.g., $^{13}C$ (1.070%), $^{18}O$ (0.205%) or $^{34}S$ (4.290%). Isotope peaks appear at distinct intensity and *m/z* value differences from the monoisotopic peak in a mass spectrum and can therefore be utilized as additional confirmation of the assigned monoisotopic sum formulae. The observed experimental data is in good agreement with the simulated fine isotopic structure, showing matching peaks of the first and second $^{13}C$ and first $^{34}S$ isotope, if applicable, in addition to the ppb-level mass error, therefore the certainty of the assignment of these uncommon elemental compositions is very high.

The highest number and relative intensity of CHNOS and CHOS compounds are found in the permafrost peat samples (Fig. 7). In general, the $OS_C$ is lower for CHNOS compounds than for CHOS compounds, while the $AI_{mod}$ is similarly distributed when comparing both compound classes. Permafrost peatland samples NOR and ROG show a higher number of aromatic OS compounds and a lower $OS_C$ compared to the boreal peatland samples FIA and FIB, which may be a result of the poor combustion conditions observed for these peat samples, leading to the emission of incomplete lignin degradation products that contain aromatic ring structures, as well as the lower degradation of biomass in permafrost peatlands.

OS compounds that are common in all datasets, including the BFS, are mostly aliphatic with a medium O/C ratio around 0.4 and H/C larger than 1.5 (Fig. 4a). Still, there is an even higher number of OS compounds that are uniquely identified in peat combustion samples, with the highest abundance in PM from permafrost peat combustion.

*Sphagnum* and other mosses, which are abundantly present at all sampling sites, are not only efficient in nitrogen-uptake, but also have a high sulfur uptake potential, which consequently increases the amounts of oxidized organosulfur compounds in living mosses and the resulting peat[56,82]. The large amount of OS compounds in moss-derived peat also leads to notable interaction of sulfur-reducing microorganisms (SRMs) with these compounds. Both, sulfate, and nitrate can act as terminal electron acceptors under anoxic conditions, and therefore SRMs can utilize sulfate to produce $CO_2$[56,83,84]. Hydrogen sulfide is formed by the reduction of sulfate and consequently forms a reactive aqueous $H_2S/S^0/H_2S_X$ system[85]. This

polysulfide system is then able to add sulfur to labile functional groups of organic matter, like carbonyl, hydroxyl, or carbon-carbon double bonds[86]. Further accumulation of sulfur in organic matter of a boreal peatland has been shown by peat core analysis from north-England[87]. It was also reported that products of dissimilatory sulfate reduction in surface peat are most likely carbon-bonded and not ester-bonded sulfur compounds[82]. Investigations of dissolved organic matter (DOM) in porewater of peatlands in northern Minnesota and Sweden have also revealed significant relative intensities of oxidized sulfur-containing compounds, indicating the presence of organosulfur species in the initial peat samples[88].

The abundance of OS species in the main peat-forming vegetation as well as interactions of them with SRM in the peat, could explain our unprecedented observation of abundant sulfur-containing organic aerosol compounds in primary boreal and Arctic peat smoldering emissions.

## Conclusions

Chemical characterization of primary boreal and Arctic peat combustion emissions by ESI 21 T FT-ICR MS revealed an extremely complex mixture of organic aerosol compounds, including high numbers of oxidized nitrogen- and sulfur-containing species. The combustion type was predominately smoldering, with some variance between the samples, highlighting the influence of the local vegetation and microbial activity on the peat composition and its combustion.

Ultrahigh field FT-ICR MS enabled the assignment of up to 45,000 monoisotopic elemental compositions in a single mass spectrum.

Arctic permafrost peat smoldering, compared to boreal peat, generated a partially similar, but less oxidized and more nitrogen- and sulfur-containing primary organic aerosol, that can easily be differentiated from the boreal peat as well as a reference sample of boreal forest floor vegetation. In the combustion experiment, an unprecedented high number of CHOS and CHNOS compounds was detected by ESI(−) in the primary organic aerosol, and compounds were verified by their fine isotopic fingerprint. The high abundance of sulfur-containing compounds is a result of the particularly high amounts of organic sulfur species in *Sphagnum*-derived peat, compared to other types of biomasses. Boreal and Arctic peat smoldering combustion therefore needs to be considered as a primary source of organic sulfur compounds in the atmosphere.

Three main molecular structure motifs were equally characterized for each compound class in all peat samples: single-core aromatic ring systems with high aromaticity and minor alkylation (island-type, combustion-derived), multicore ring systems with medium to low aromaticity and high degree of alkylation (archipelago-type, lignin decomposition derived) as well as aliphatic-like structures without an aromatic ring. Island-type compounds were most abundantly observed, and these compounds may have an important contribution to peat aerosol-induced light absorption in the atmosphere.

In the future, the application of MS based isolation and fragmentation experiments could help further improve the understanding of general structural motifs in peat organic aerosol as well as the location of nitrogen and sulfur in the molecules.

## Methods

### Sampling sites and laboratory burning experiments

Five biomass samples were collected at four locations in northern continental Europe (Finland and Russia) and at one location further north on Svalbard (a Norwegian High-Arctic Archipelago) (Fig. 1). Two peat samples originate from Finland, more precisely from the peatlands Lakkasuo (FIA, 61°47'21.6"N 24°18'35.9"E) and Siikaneva (FIB, 61°49'28.0"N 24°08'25.8"E), approximately 10 km away from each other. Two other peat samples originate from permafrost peatlands on Svalbard (Alkehornet), Norway (NOR, 78°13'00.0"N 13°45'00.0"E) and in Rogovaya, Russia (ROG, 66°33'10.2"N 60°37'57.3"E). Additionally, a sample representing the BFS in Evo (BFS, Finland: 61°11'48.8"N 25°05'39.2"E) was analyzed to characterize potential differences of combustion products from boreal forest fires compared to boreal and Arctic peat fires. The top 30 cm of peat was collected with a Russian peat corer (diameter 7.5 cm) from the studied peatlands (FIA, FIB, NOR, ROG). From boreal forest (BFS), the samples (diameter of the sample 21 cm and height 10 cm) containing vegetation, floor (litter, and soil organic layer (all horizons that might be affected during the surface fire) were collected from 90-year-old Scots pine (*Pinus sylvestris L.*) forest. All samples were stored under dark and dry conditions until the combustion experiment.

The initial composition of biomass that forms the peat is determined by local vegetation. The vegetation, on the other hand varies according to, for instance, the local topography, water table, acidity, and climate. The peat composition and environmental conditions in turn affect the species composition and microbial activity of microorganisms. Both Finnish peat samples (FIA, FIB) were collected from ombrotrophic boreal peatlands characterized by vegetation dominated by *Sphagnum* moss cover as well as sedges and some small shrubs and birch trees. In contrast, the samples ROG and NOR originate from the active layer of Arctic permafrost peatlands that experience lower peat formation due to the harsher climatic conditions. The main vegetation at the minerotrophic ROG sampling site is dominated by sedges and, to a lesser extent, Sphagnum mosses and some shrubs. The vegetation at the Svalbard study site (NOR) is characterized as herbaceous moss tundra. Notably, this peatland (NOR) is near a bird cliff which has a strong fertilizing effect, leading to an increased nitrogen content in the peat[57]. Naturally occurring wildfires have been reported for boreal peatlands in Finland and permafrost peatlands[89,90], but not for Svalbard. Still, peat from this location can serve as an example of unique peat compositions found in Arctic peatlands, which are exposed to higher wildfire risks in the future[19] and have already burned in western Greenland[91] as well as highlighting the effect of the fuel chemical composition on resulting organic aerosol composition.

Open BB was conducted at the ILMARI laboratory of the University of Eastern Finland (www.uef.fi/ilmari). Each peat sample to be burned weighed 50 g whereas the BFS sample mass was 349 g. For the experiments, the biomass sample was inserted in a steel cage, which was placed on a concave plate surrounded by metal mesh walls. On top of the biomass sample was a hood, which was connected to a chimney equipped with a flue gas fan, which draws the formed exhaust gases. In the hood the exhaust gases become diluted on average by a factor of 1:259 to 1:1261 depending on the combustion rate, which varied between the different biomasses. The biomass samples were ignited using a heating element located within the sample. This element was supplied with constant power and was deactivated either immediately after visible flames or one minute after ignition to ensure the flame did not extinguish. During heating, the biomass initially began to smolder before fully igniting in flames. The ignition process before flames took 4 min for the NOR sample and 3 min for other samples, as described in Supplementary Table 1.

Modified combustion efficiency (MCE) was calculated based on background corrected FTIR data of carbon monoxide (ΔCO) measured by Fourier Transform Infrared Spectroscopy (FTIR, DX4000, Gasmet) and carbon dioxide ($\Delta CO_2$) measured by FTIR and an NDIR-based trace level $CO_2$ gas analyzer (Siemens, ULTRAMAT 23):

$$\mathrm{MCE} = \frac{\Delta\ \mathrm{CO_2}}{\Delta\ \mathrm{CO_2} + \Delta\ \mathrm{CO}} \quad (1)$$

The peat combustion experiment was considered to start when flue gas CO concentration reached 5 ppm and to end likewise when CO concentration dropped below 5 ppm. The BFS experiment was started when CO concentration reached 10 ppm and was stopped at CO concentration of 24 ppm.

Samples of total suspended PM from the flue gas were collected on 90 mm diameter quartz fiber filters (Pallflex Tissuquartz) using a stainless-steel filter holder (Geotech, model SS90, Denver, Colorado, USA) and a sampling flow rate of 90 l $min^{-1}$ for 12–55 min depending on the duration of the combustion (Supplementary Table 1).

Thermal analysis (TG 209 cell thermobalance, Netzsch, Selb, Germany) was conducted by applying a temperature ramp of 10 K $min^{-1}$ in the range of 30–600 °C on 7–22 mg of cryo-milled peat aliquots under atmospheric conditions.

The carbon and nitrogen contents of the original peat samples were determined with a Flash 2000 Organic Elemental Analyzer (Thermo Fisher).

### Thermo-optical carbon analysis (TOCA) and filter extraction

For direct analysis of QFF samples, a thermal-optical carbon analyzer (TOCA; Model 2001, DRI, USA) was used to determine organic and elemental carbon (OC, EC) according to the IMPROVE_A protocol[92], using laser transmittance at 635 nm for separation of pyrolytic OC from EC.

A 4.5 $cm^2$ section of each QFF was extracted in a pre-baked glass vial by the addition of 4 ml Methanol/Dichloromethane (1/1 v%, LC-MS grade) and ultra-sonication for 30 min in an ice-chilled water bath. After a final filtration step (0.22 µm PTFE membrane, Sartorius, Goettingen, Germany) the extracts were stored in a freezer at −25 °C until analysis. Shortly before measurement, each extract was diluted by methanol to approximately the same concentration of 200 µg OC $ml^{-1}$, based on OC mass determined using TOCA (Supplementary Table 2).

### Ultrahigh-resolution mass spectrometry

ESI coupled to FT-ICR MS were conducted on a custom-built hybrid linear ion trap FT-ICR mass spectrometer equipped with a 21 T superconducting magnet, located at the National High Magnetic Field Laboratory in Tallahassee, Florida[49]. The extracts were analyzed by direct-infusion microelectrospray ionization[93] via a 50 µm i.d. fused silica emitter at a flow rate of 0.55 µL $min^{-1}$ and a voltage of −3.5/3.0 kV in positive and negative ionization mode, respectively. Time domain transients of 3.2 s were conditionally co-added (200–550 Scans, dependent on single scan intensity variation) to achieve comparable total ion abundances. $1.5 \times 10^6$ charges were externally accumulated and transferred to the ICR cell for analysis. All datasets were recorded as single measurements, which is a common practice because of the high precision of the instrument. All FT-ICR mass spectra files, calibration lists, and assigned elemental compositions are publicly available via the Open Science Framework at https://doi.org/10.17605/OSF.IO/4PJFC[94].

### Data analysis and sum formula assignment

Predator software was used for processing of coadded time-domain transients, including phasing, Fourier transformation, peak picking (peaks greater 6 than six times the baseline root-mean-square noise at *m/z* 400), and initial mass spectral calibration. Final mass calibration of exported peak lists was carried out by Python-based notebooks (PyC2MC)[95], based on selected intensive Kendrick mass series covering the whole mass range and consequent walking calibration based on the created calibration lists for each sample. Formula assignment was carried out by the same software based on stepwise iterative sum formula assignment of $C_cH_hN_nO_oS_sP_pNa_{0\text{-}1}$ (Supplementary Table 3) in the range of 180–1200 Da, with a maximum error of 200 ppb and additional automated confirmation via isotope pattern comparison ($^{13}C_1$) as well as manual confirmation of selected sulfur-containing compounds ($^{34}S_1$, $^{13}C_2$). After calibration and sum formula assignment the resulting mean error averaged for all datasets was 36.1 ± 3.3 ppb and a root-mean square error of 52.4 ± 4.3 ppb. Data visualization and molecular property calculations were assisted by MatLab (R2023a) and are described in detail elsewhere[96,97]. Double bond equivalents (DBE), modified aromaticity index ($AI_{mod}$), saturation vapor pressure (log(C*), coefficients $b_x$ from Li Y. et al. 2012 (Supplementary Table 4)[59], and the average carbon oxidation state ($OS_C$) of CHO compounds were calculate based on the assigned neutral elemental composition (excluding P):

$$\mathrm{DBE} = c - \frac{h+n}{2} + 1 \tag{2}$$

$$AI_{\mathrm{mod}} = \frac{1 + c - 0.5 * o - s - 0.5 * (h+n)}{c - 0.5 * o - s - n} \tag{3}$$

$$\log_{10} C^* = \left(n_C^0 - c\right) b_C - o b_O - 2\frac{c*o}{c+o} b_{CO} - n b_N - s b_S \tag{4}$$

$$OS_C = 2 * \frac{o}{c} - \frac{h}{c}. \tag{5}$$

Simulation of the fine isotopic structure of selected elemental compositions (absorption mode, semikaiser apodization, 2 times zero-filled) was carried out by the software Peak-by-Peak (Base Edition, Version 2023.5.0.b5, Spectroswiss, Switzerland).

### Reporting summary

Further information on research design is available in the Nature Portfolio Reporting Summary linked to this article.

## Data availability

All FT-ICR mass spectra files and assigned elemental compositions are publicly available via the Open Science Framework at https://doi.org/10.17605/OSF.IO/4PJFC.

Received: 6 October 2023; Accepted: 4 March 2024;
Published online: 16 March 2024

## References

1. Turetsky, M. R. et al. Global vulnerability of peatlands to fire and carbon loss. *Nat. Geosci.* **8**, 11–14 (2015).
2. Kohlenberg, A. J., Turetsky, M. R., Thompson, D. K., Branfireun, B. A. & Mitchell, C. P. J. Controls on boreal peat combustion and resulting emissions of carbon and mercury. *Environ. Res. Lett.* **13**, 35005 (2018).
3. IPCC. Climate change and land. An IPCC special report on climate change, desertification, land degradation, sustainable land management, food security, and greenhouse gas fluxes in terrestrial ecosystems: summary for policymakers (Intergovernmental Panel on Climate Change, [Geneva], 2019).
4. Moore, P. D. Ecological and hydrological aspects of peat formation. *Spec. Publ.* **32**, 7–15 (1987).
5. Fewster, R. E. et al. Imminent loss of climate space for permafrost peatlands in Europe and Western Siberia. *Nat. Clim. Change* **12**, 373–379 (2022).
6. D. W. van Krevelen. Graphical-statistical method for the study of structure and reaction processes of coal. *Fuel* **29**, 269–284 (1950).
7. Hu, Y., Fernandez-Anez, N., Smith, T. E. L. & Rein, G. Review of emissions from smouldering peat fires and their contribution to regional haze episodes. *Int. J. Wildland Fire* **27**, 293 (2018).
8. Hugelius, G. et al. Large stocks of peatland carbon and nitrogen are vulnerable to permafrost thaw. *PNAS* **117**, 20438–20446 (2020).
9. Jiao, Y. et al. Volatile organic compound release across a permafrost-affected peatland. *Geoderma* **430**, 116355 (2023).
10. Descals, A. et al. Unprecedented fire activity above the Arctic Circle linked to rising temperatures. *Science (New York, N.Y.)* **378**, 532–537 (2022).
11. Fujii, Y. et al. Characteristics of carbonaceous aerosols emitted from peatland fire in Riau, Sumatra, Indonesia (2): Identification of organic compounds. *Atmos. Environ.* **110**, 1–7 (2015).
12. Langmann, B., Duncan, B., Textor, C., Trentmann, J. & van der Werf, G. R. Vegetation fire emissions and their impact on air pollution and climate. *Atmos. Environ.* **43**, 107–116 (2009).
13. Poulter, B., Christensen, N. L. & Halpin, P. N. Carbon emissions from a temperate peat fire and its relevance to interannual variability of trace atmospheric greenhouse gases. *J. Geophys. Res.* **111**; https://doi.org/10.1029/2005JD006455 (2006).

14. Pearson, R. G. et al. Shifts in Arctic vegetation and associated feedbacks under climate change. *Nat. Clim. Change* **3**, 673–677 (2013).
15. Popovicheva, O. B., Engling, G., Ku, I.-T., Timofeev, M. A. & Shonija, N. K. Aerosol emissions from long-lasting smoldering of boreal peatlands: Chemical composition, markers, and microstructure. *Aerosol. Air Qual. Res.* **19**, 484–503 (2019).
16. Witze, A. The Arctic is burning like never before—and that's bad news for climate change. *Nature* **585**, 336–337 (2020).
17. Sim, T. G. et al. Regional variability in peatland burning at mid-to high-latitudes during the Holocene. *Quat. Sci. Rev.* **305**, 108020 (2023).
18. McCarty, J. L., Smith, T. E. L. & Turetsky, M. R. Arctic fires re-emerging. *Nat. Geosci* **13**, 658–660 (2020).
19. Irannezhad, M., Liu, J., Ahmadi, B. & Chen, D. The dangers of Arctic zombie wildfires. *Science* **369**, 1171 (2020).
20. Stracher, G. B., Prakash, A., Rein, G. (ed.). Coal and peat fires: a global perspective (Elsevier, 2015).
21. Rein, G. Smouldering fires and natural fuels. *In:* Fire phenomena and the earth system, edited by Belcher, C. M. (John Wiley & Sons, Oxford, pp. 15–33, 2013)
22. Scholten, R. C., Jandt, R., Miller, E. A., Rogers, B. M. & Veraverbeke, S. Overwintering fires in boreal forests. *Nature* **593**, 399–404 (2021).
23. Lin, S., Liu, Y. & Huang, X. Climate-induced Arctic-boreal peatland fire and carbon loss in the 21st century. *Sci. Total Environ.* **796**, 148924 (2021).
24. Chakrabarty, R. K. et al. Brown carbon aerosols from burning of boreal peatlands: microphysical properties, emission factors, and implications for direct radiative forcing. *Atmos. Chem. Phys.* **16**, 3033–3040 (2016).
25. Rappold, A. G. et al. Peat bog wildfire smoke exposure in rural North Carolina is associated with cardiopulmonary emergency department visits assessed through syndromic surveillance. *Environ. Health Perspect.* **119**, 1415–1420 (2011).
26. Tinling, M. A., West, J. J., Cascio, W. E., Kilaru, V. & Rappold, A. G. Repeating cardiopulmonary health effects in rural North Carolina population during a second large peat wildfire. *Environ. Health* **15**, 12 (2016).
27. Martin, B. L. et al. Peat smoke inhalation alters blood pressure, baroreflex sensitivity, and cardiac arrhythmia risk in rats. *J. Toxicol. Environ. Health Part A* **83**, 748–763 (2020).
28. Kim, Y. H. et al. Mutagenicity and lung toxicity of smoldering vs. flaming emissions from various biomass fuels: implications for health effects from wildland fires. *Environ. Health Perspect.* **126**, 17011 (2018).
29. Laskin, A., Laskin, J. & Nizkorodov, S. A. Chemistry of atmospheric brown carbon. *Chem. Rev.* **115**, 4335–4382 (2015).
30. Lyu, M. et al. Unraveling the complexity of atmospheric brown carbon produced by smoldering boreal peat using size-exclusion chromatography with selective mobile phases. *Environ. Sci. Atmos.* **1**, 241–252 (2021).
31. Budisulistiorini, S. H. et al. Light-absorbing brown carbon aerosol constituents from combustion of indonesian peat and biomass. *Environ. Sci. Technol.* **51**, 4415–4423 (2017).
32. Sedlacek III, A. J. et al. Formation and evolution of tar balls from northwestern US wildfires. *Atmos. Chem. Phys.* **18**, 11289–11301 (2018).
33. Hansen, A. M. K. et al. Hygroscopic properties and cloud condensation nuclei activation of limonene-derived organosulfates and their mixtures with ammonium sulfate. *Atmos. Chem. Phys.* **15**, 14071–14089 (2015).
34. Zhang, Y. et al. Joint impacts of acidity and viscosity on the formation of secondary organic aerosol from isoprene epoxydiols (IEPOX) in phase separated particles. *ACS Earth Space Chem.* **3**, 2646–2658 (2019).
35. Riva, M. et al. Increasing isoprene epoxydiol-to-inorganic sulfate aerosol ratio results in extensive conversion of inorganic sulfate to organosulfur forms: implications for aerosol physicochemical properties. *Environ. Sci. Technol.* **53**, 8682–8694 (2019).
36. Hallquist, M. et al. The formation, properties and impact of secondary organic aerosol: current and emerging issues. *Atmos. Chem. Phys.* **9**, 5155–5236 (2009).
37. Bowman, A. P. et al. Ultra-high mass resolving power, mass accuracy, and dynamic range MALDI mass spectrometry imaging by 21-T FT-ICR MS. *Anal. Chem.* **92**, 3133–3142 (2020).
38. Roth, H. K. et al. Enhanced speciation of pyrogenic organic matter from wildfires enabled by 21 T FT-ICR mass spectrometry. *Anal. Chem.* **94**, 2973–2980 (2022).
39. Young, R. B. et al. PFAS analysis with ultrahigh resolution 21T FT-ICR MS: suspect and nontargeted screening with unrivaled mass resolving power and accuracy. *Environ. Sci. Technol.* **56**, 2455–2465 (2022).
40. Putman, J. C. et al. Probing aggregation tendencies in asphaltenes by gel permeation chromatography. Part 2: online detection by fourier transform ion cyclotron resonance mass spectrometry and inductively coupled plasma mass spectrometry. *Energy Fuels* **34**, 10915–10925 (2020).
41. Ijaz, A., Kew, W., China, S., Schum, S. K. & Mazzoleni, L. R. Molecular characterization of organophosphorus compounds in wildfire smoke using 21-T Fourier transform-ion cyclotron resonance mass spectrometry. *Anal. Chem.* **94**, 14537–14545 (2022).
42. Akagi, S. K. et al. Emission factors for open and domestic biomass burning for use in atmospheric models. *Atmos. Chem. Phys.* **11**, 4039–4072 (2011).
43. Andersen, R., Chapman, S. J. & Artz, R. Microbial communities in natural and disturbed peatlands: a review. *Soil Biol. Biochem.* **57**, 979–994 (2013).
44. Atlas, R. M. Petroleum biodegradation and oil spill bioremediation. *Mar. Pollut. Bull.* **31**, 178–182 (1995).
45. Burgoyne, J. H., Tang, T. L. & Newitt, D. M. The combustion of aromatic and alicyclic hydrocarbons. III. Ignition and cool-flame characteristics. *Proc. R. Soc. Lond. A* **174**, 379–393 (1940).
46. Kourtchev, I. et al. The use of polar organic compounds to estimate the contribution of domestic solid fuel combustion and biogenic sources to ambient levels of organic carbon and PM2.5 in Cork Harbour, Ireland. *Sci. Total Environ.* **409**, 2143–2155 (2011).
47. Limbach, P. A., Grosshans, P. B. & Marshall, A. G. Experimental determination of the number of trapped ions, detection limit, and dynamic range in Fourier transform ion cyclotron resonance mass spectrometry. *Anal. Chem.* **65**, 135–140 (1993).
48. Bahureksa, W. et al. Improved dynamic range, resolving power, and sensitivity achievable with FT-ICR mass spectrometry at 21 T reveals the hidden complexity of natural organic matter. *Anal. Chem.* **94**, 11382–11389 (2022).
49. Smith, D. F., Podgorski, D. C., Rodgers, R. P., Blakney, G. T. & Hendrickson, C. L. 21 tesla FT-ICR mass spectrometer for ultrahigh-resolution analysis of complex organic mixtures. *Anal. Chem.* **90**, 2041–2047 (2018).
50. Vladimirov, G. et al. Fourier transform ion cyclotron resonance mass resolution and dynamic range limits calculated by computer modeling of ion cloud motion. *J. Am. Soc. Mass Spectrom.* **23**, 375–384 (2012).
51. Nagao, T. et al. Power of isotopic fine structure for unambiguous determination of metabolite elemental compositions: in silico evaluation and metabolomic application. *Anal. Chim. Acta* **813**, 70–76 (2014).
52. Hendrickson, C. L. et al. 21 tesla fourier transform ion cyclotron resonance mass spectrometer: a national resource for ultrahigh resolution mass analysis. *J. Am. Soc. Mass Spectrom.* **26**, 1626–1632 (2015).

53. Zhong, S. et al. Impact of biogenic secondary organic aerosol (SOA) loading on the molecular composition of wintertime PM 2.5 in urban Tianjin: an insight from Fourier transform ion cyclotron resonance mass spectrometry. *Atmos. Chem. Phys.* **23**, 2061–2077 (2023).
54. Simoneit, B. R. Biomass burning — a review of organic tracers for smoke from incomplete combustion. *Appl. Geochem.* **17**, 129–162 (2002).
55. Brege, M. et al. Molecular insights on aging and aqueous-phase processing from ambient biomass burning emissions-influenced Po Valley fog and aerosol. *Atmos. Chem. Phys.* **18**, 13197–13214 (2018).
56. AminiTabrizi, R. et al. Controls on soil organic matter degradation and subsequent greenhouse gas emissions across a permafrost thaw gradient in Northern Sweden. *Front. Earth Sci*. **8**, 557961 (2020).
57. Juselius, T. et al. Newly initiated carbon stock, organic soil accumulation patterns and main driving factors in the High Arctic Svalbard, Norway. *Sci. Rep.* **12**, 4679 (2022).
58. Donahue, N. M., Epstein, S. A., Pandis, S. N. & Robinson, A. L. A two-dimensional volatility basis set: 1. organic-aerosol mixing thermodynamics. *Atmos. Chem. Phys.* **11**, 3303–3318 (2011).
59. Li, Y., Pöschl, U. & Shiraiwa, M. Molecular corridors and parameterizations of volatility in the chemical evolution of organic aerosols. *Atmos. Chem. Phys.* **16**, 3327–3344 (2016).
60. Yatavelli, R. L. N. et al. Emissions and partitioning of intermediate-volatility and semi-volatile polar organic compounds (I/SV-POCs) during laboratory combustion of boreal and sub-tropical peat. *Aerosol Sci. Eng.* **1**, 25–32 (2017).
61. Cho, Y., Kim, Y. H. & Kim, S. Planar limit-assisted structural interpretation of saturates/aromatics/resins/asphaltenes fractionated crude oil compounds observed by Fourier transform ion cyclotron resonance mass spectrometry. *Anal. Chem.* **83**, 6068–6073 (2011).
62. Rüger, C. P., Sklorz, M., Schwemer, T. & Zimmermann, R. Characterisation of ship diesel primary particulate matter at the molecular level by means of ultra-high-resolution mass spectrometry coupled to laser desorption ionisation–comparison of feed fuel, filter extracts and direct particle measurements. *Anal. Bioanal. Chem.* **407**, 5923–5937 (2015).
63. Chacón-Patiño, M. L., Rowland, S. M. & Rodgers, R. P. Advances in asphaltene petroleomics. part 1: asphaltenes are composed of abundant island and archipelago structural motifs. *Energy Fuels* **31**, 13509–13518 (2017).
64. Neumann, A., Chacón-Patiño, M. L., Rodgers, R. P., Rüger, C. P. & Zimmermann, R. Investigation of island/single-core- and archipelago/multicore-enriched asphaltenes and their solubility fractions by thermal analysis coupled with high-resolution fourier transform ion cyclotron resonance mass spectrometry. *Energy Fuels* **35**, 3808–3824 (2021).
65. Martens, P. et al. Brown coal and logwood combustion in a modern heating appliance: the impact of combustion quality and fuel on organic aerosol composition. *Environ. Sci. Technol.* **57**, 5532–5543 (2023).
66. Wentzel, A., Ellingsen, T. E., Kotlar, H.-K., Zotchev, S. B. & Throne-Holst, M. Bacterial metabolism of long-chain n-alkanes. *Appl. Microbiol. Biotechnol.* **76**, 1209–1221 (2007).
67. Rodgers, R. P. et al. Combating selective ionization in the high resolution mass spectral characterization of complex mixtures. *Faraday Discuss.* **218**, 29–51 (2019).
68. Kosyakov, D. S. et al. Peat burning—an important source of pyridines in the earth atmosphere. *Environ. Pollut.* **266**, 115109 (2020).
69. Laskin, A., Smith, J. S. & Laskin, J. Molecular characterization of nitrogen-containing organic compounds in biomass burning aerosols using high-resolution mass spectrometry. *Environ. Sci. Technol.* **43**, 3764–3771 (2009).
70. Çelik, G., Beil, S., Stolte, S. & Markiewicz, M. Environmental hazard screening of heterocyclic polyaromatic hydrocarbons: physicochemical data and in silico models. *Environ. Sci. Technol.* **57**, 570–581 (2023).
71. Lin, P. et al. Molecular characterization of brown carbon in biomass burning aerosol particles. *Environ. Sci. Technol.* **50**, 11815–11824 (2016).
72. Fritz, C., Lamers, L. P. M., Riaz, M., van den Berg, L. J. L. & Elzenga, T. J. T. M. Sphagnum mosses–masters of efficient N-uptake while avoiding intoxication. *PLoS One* **9**, e79991 (2014).
73. Li, C. et al. Formation of secondary brown carbon in biomass burning aerosol proxies through NO3 radical reactions. *Environ. Sci. Technol.* **54**, 1395–1405 (2020).
74. Ye, C. et al. Low-NO-like oxidation pathway makes a significant contribution to secondary organic aerosol in polluted urban air. *Environ. Sci. Technol.* **57**, 13912–13924 (2023).
75. Decker, Z. C. J. et al. Nighttime and daytime dark oxidation chemistry in wildfire plumes: an observation and model analysis of FIREX-AQ aircraft data. *Atmos. Chem. Phys.* **21**, 16293–16317 (2021).
76. Brüggemann, M. et al. Organosulfates in ambient aerosol: state of knowledge and future research directions on formation, abundance, fate, and importance. *Environ. Sci. Technol.* **54**, 3767–3782 (2020).
77. Wang, X. K. et al. Molecular characterization of atmospheric particulate organosulfates in three megacities at the middle and lower reaches of the Yangtze River. *Atmos. Chem. Phys.* **16**, 2285–2298 (2016).
78. Ye, Y. et al. Detection of organosulfates and nitrooxy-organosulfates in Arctic and Antarctic atmospheric aerosols, using ultra-high resolution FT-ICR mass spectrometry. *Sci. Total Environ.* **767**, 144339 (2021).
79. Riva, M. et al. Chemical characterization of organosulfates in secondary organic aerosol derived from the photooxidation of alkanes. *Atmos. Chem. Phys.* **16**, 11001–11018 (2016).
80. Passananti, M. et al. Organosulfate formation through the heterogeneous reaction of sulfur dioxide with unsaturated fatty acids and long-chain alkenes. *Angew. Chem. Int. Ed. Engl.* **55**, 10336–10339 (2016).
81. Xie, Q. et al. Increase of nitrooxy organosulfates in firework-related urban aerosols during Chinese New Year's Eve. *Atmos. Chem. Phys.* **21**, 11453–11465 (2021).
82. Novak, M. & Wieder, R. K. Inorganic and organic sulfur profiles in nine Sphagnum peat bogs in the United States and Czechoslovakia. *Water Air Soil Pollut.* **65**, 353–369 (1992).
83. Muyzer, G. & Stams, A. J. M. The ecology and biotechnology of sulphate-reducing bacteria. *Nat. Rev. Microbiol.* **6**, 441–454 (2008).
84. Pester, M., Knorr, K.-H., Friedrich, M. W., Wagner, M. & Loy, A. Sulfate-reducing microorganisms in wetlands—fameless actors in carbon cycling and climate change. *Front. Microbiol.* **3**, 72 (2012).
85. Orr, W. L. & Sinninghe Damsté, J. S. Geochemistry of Sulfur in Petroleum Systems. *In:* Geochemistry of sulfur in fossil fuels, edited by Orr, W. L. & White, C. M. (American Chemical Society, Washington, DC, Vol. 429, pp. 2–29. 1990)
86. LaLonde, R. T. et al. Variable reaction pathways for the action of polysulfide on Michael acceptors. *J. Org. Chem.* **50**, 85–91 (1985).
87. Boothroyd, I. M. et al. Sulfur constraints on the carbon cycle of a blanket bog peatland. *J. Geophys. Res.: Biogeosci*. **126**, e2021JG006435 (2021).
88. Tfaily, M. M., Hodgkins, S., Podgorski, D. C., Chanton, J. P. & Cooper, W. T. Comparison of dialysis and solid-phase extraction for isolation and concentration of dissolved organic matter prior to Fourier transform ion cyclotron resonance mass spectrometry. *Anal. Bioanal. Chem.* **404**, 447–457 (2012).
89. Mathijssen, P. J. H. et al. Lateral expansion and carbon exchange of a boreal peatland in Finland resulting in 7000 years of positive radiative forcing. *J. Geophys. Res. Biogeosci.* **122**, 562–577 (2017).
90. Gibson, C. M. et al. Wildfire as a major driver of recent permafrost thaw in boreal peatlands. *Nat. Commun.* **9**, 3041 (2018).

91. Evangeliou, N. et al. Open fires in Greenland in summer 2017: transport, deposition and radiative effects of BC, OC and BrC emissions. *Atmos. Chem. Phys.* **19**, 1393–1411 (2019).
92. Chow, J. C. et al. The IMPROVE_A temperature protocol for thermal/optical carbon analysis: maintaining consistency with a long-term database. *J. Air Waste Manag. Assoc.* **57**, 1014–1023 (2007).
93. Emmett, M. R., White, F. M., Hendrickson, C. L., Shi, S. D. & Marshall, A. G. Application of micro-electrospray liquid chromatography techniques to FT-ICR MS to enable high-sensitivity biological analysis. *J. Am. Soc. Mass Spectrom.* **9**, 333–340 (1998).
94. Chacon-Patino, M. L. Unraveling the molecular complexity of boreal and arctic peat burning particulate matter by 21 T fourier transform ion cyclotron resonance mass spectrometry, https://doi.org/10.17605/OSF.IO/4PJF (OSF, 2023).
95. International complex matrices molecular characterization. PyC2MC. Available at https://git.univ-pau.fr/ic2mc/pyc2mc (2023).
96. Schneider, E. et al. Molecular characterization of water-soluble aerosol particle extracts by ultrahigh-resolution mass spectrometry: observation of industrial emissions and an atmospherically aged wildfire Plume at Lake Baikal. *ACS Earth Space Chem.* **6**, 1095–1107 (2022).
97. Schneider, E. et al. Humic-like substances (HULIS) in ship engine emissions: molecular composition effected by fuel type, engine mode, and wet scrubber usage. *Environ. Sci. Technol*. **57**, 13948–13958 (2023).


## Acknowledgements

This work was supported by the German Research Foundation (DFG) under grant ZI 764/24-1 and the Research Council of Finland (grant 341597). A portion of the work was performed at the National High Magnetic Field Laboratory ICR User Facility, which is supported by the National Science Foundation Division of Chemistry and Division of Material Research through DMR-1644779 and the State of Florida. H.C. acknowledges funding from the Helmholtz Association (HGF) by the Helmholtz International Laboratory aeroHEALTH (InterLabs-0005). The authors thank the DFG for funding the Bruker FT-ICR MS (INST 264/56). M.M.R. acknowledges support received from Arctic Avenue and the Research Council of Finland projects 355871 and 341271.

## Author contributions

E.S. methodology, investigation, formal analysis, writing—original draft, visualization, writing—review & editing; C.P.R.: methodology, software, resources, writing—review & editing, supervision, project administration; M.L.C.P.: investigation, recourses, review & editing; M.S.: investigation, data curation; M.M.R.: conceptualization, investigation, review & editing; M.I.: investigation, review & editing; K.K.: conceptualization, investigation, writing—review & editing; O.S.: conceptualization, investigation, review & editing, supervision, resources, funding acquisition; H.C.: conceptualization, writing—review & editing, supervision, project administration; R.Z.: resources, writing—review & editing, funding acquisition.

## Funding

Open Access funding enabled and organized by Projekt DEAL.

## Competing interests

The authors declare no competing interests.

## Additional information

**Supplementary information** The online version contains supplementary material available at https://doi.org/10.1038/s43247-024-01304-y.

**Correspondence** and requests for materials should be addressed to Christopher P. Rüger or Hendryk Czech.

**Peer review information** *Communications Earth & Environment* thanks the anonymous reviewers for their contribution to the peer review of this work. Primary Handling Editors: Keiichiro Hara, Clare Davis and Martina Grecequet. A peer review file is available.